Available online at www.sciencedirect.com
ScienceDirect
Journal of the European Ceramic Society 29 (2009) 1679–1686
www.elsevier.com/locate/jeurceramsoc

Synthesis and sintering of a monazite–brabantite solid solution ceramics using metaphosphate

B. Glorieux [a,*], J.M. Montel [b], M. Matecki [c]

[a] *Procédés, Matériaux et Energie Solaire (PROMES), CNRS-UPR 8521, Rambla de la Thermodynamique, Technosud, 66100 Perpignan, France*
[b] *Laboratoire des Mécanismes et Transferts en Géologie (LMTG), UMR 5563, 14 avenue Edouard Belin, 31400 Toulouse, France*
[c] *Procédés, Matériaux et Energie Solaire (PROMES), CNRS-UPR 8521, 7 Rue du Four Solaire 66120 Font-Romeu, France*

Received 18 February 2008; received in revised form 17 September 2008; accepted 8 October 2008
Available online 26 November 2008

Abstract

In order to improve monazite-based ceramics, to be used as actinides waste-form, a procedure for synthesis and sintering of a monazite–brabantite solid solution (ssMB) using metaphosphate $La(PO_3)_3$ is described. Using $LaPO_4$, CeO_2, ThO_2, $CaCO_3$ and $La(PO_3)_3$ as precursors, the gaseous emissions are strongly reduced, compared to a process using $(NH_4)H_2PO_4$. Detailed dilatometric studies show sintering of that product is a two-steps process: coalescence and boundary diffusion. From X-ray diffraction, electron microprobe analyses, SEM observation, dilatometric study and TG–DTA, the reaction scheme is identified and the thermal treatment for synthesis and sintering is optimized to obtain homogeneous, dense, reproducible and well-crystallized pellets of $La_{0.73}Ce_{0.09}Th_{0.09}Ca_{0.09}PO_4$ and $La_{0.91}Ce_{0.09}PO_4$.

Keywords: A. Sintering; B. Grain size; C. Thermal properties; E. Nuclear applications; Phosphates

1. Introduction

Monazite–brabantite solid solution (ssMB) has been proposed as waste-form for minor actinides (Np, Am, Cm) obtained by reprocessing of spent fuel.[1–5] This compound is based on monazite, a natural light rare earth orthophosphate, which incorporates significant amounts of thorium and uranium.[6–11] This mineral is chemically durable,[12–17] and displays an interesting behavior under irradiation.[18–21] In order to evaluate the actual potential of this product, several programs dealing with synthesis, sintering, and leaching of monazite are presently in progress.[22–27]

Montel et al.[28] demonstrated that it is possible to synthesize and sinter ssMB with a procedure suitable for an industrial process under a radioactive environment. The chosen composition, $La_{0.73}Ce_{0.09}Ca_{0.09}Th_{0.09}PO_4$ simulates ceramics with 10 wt% of trivalent (Ce^{3+} surrogate for Pu^{3+}, Am^{3+} and Cm^{3+}) or tetravalent (Th^{4+} surrogate for Np^{4+}) actinides. In this scheme, calcium is used as a charge-balancing element for thorium.[29] Cerium and plutonium are incorporated as a trivalent ion, by reduction of the dioxide at high temperature[26], as determined by NMR[30] and XPS,[31] EXAFS and XPS.[29,32]

However, this process uses ammonium dihydrogenophosphate, which produces ammonia and water during the thermal treatment. The aim of this paper is to present an alternative path with a reduced gas production. Since the process must be compatible with nuclear facilities, we used a solid-state reaction and not sol–gel reaction, mixer mill (as Terra et al.[27]) and not attrition mill, and room temperature uniaxial pressing and not hot-pressing.

The experimental and analytical details are fundamentally similar to Ref. 28, then only briefly described hereafter.

2. Experimental

2.1. Formulation, synthesis procedure

As in Montel et al.,[28] cerium and thorium are used as surrogates for actinides respectively in their tri- and tetravalent oxidation state. The desired composition is $La_{0.73}Ce_{0.09}Th_{0.09}Ca_{0.09}PO_4$.

* Corresponding author. Tel.: +33 5 40 00 62 95; fax: +33 5 40 00 27 61.
E-mail address: glorieux@icmcb-bordeaux.cnrs.fr (B. Glorieux).

0955-2219/$ – see front matter © 2008 Elsevier Ltd. All rights reserved.
doi:10.1016/j.jeurceramsoc.2008.10.004

Many publications[25–27,33–40] report various ways to synthesize such materials. In this work, we wanted to develop a high-temperature solid-state reaction (hydrous reactions would increase the risk of criticality because water is an efficient neutron moderator) with a limited gas production. With the equipment used by Montel et al.[28] (a Retsch MM200 mixer mill, high-temperature furnace and a manual hydraulic uniaxial press), we investigated a process in which the sources of phosphate are lanthanum metaphosphate, $La(PO_3)_3$, and lanthanum phophate (monazite), $LaPO_4$, instead of $(NH_4)H_2PO_4$.

The reaction, which produces only a small amount of CO_2 and O_2, is then

$$0.595LaPO_4 + 0.09CeO_2 + 0.09ThO_2 + 0.09CaCO_3 + 0.135La(PO_3)_3 \Rightarrow La_{0.73}Ce_{0.09}Th_{0.09}Ca_{0.09}PO_4 + 0.09CO_2 + 0.0225O_2 \quad (1)$$

When thorium, for safety reasons, could not be used we also studied another reaction:

$$0.865LaPO_4 + 0.09CeO_2 + 0.045La(PO_3)_3 \rightarrow La_{0.91}Ce_{0.09}PO_4 + 0.0225O_2 \quad (2)$$

2.2. Analytical procedure

2.2.1. XRD

The X-ray patterns are obtained with a CPS 120 Innel CPS 120, as in Ref. 28, and with an automated Philips PW 1820 diffractometer working with the Ni filtered Cu Kα radiation (λ = 1.54184 Å). The patterns were compared to the PDF database using XPERT Philips software; the spectra were smoothed using a reverse FFT routine and the peaks were identified by a second derivative technique. The cell parameters were calculated using Rietveld refinement with the FullProf software.[41]

2.2.2. Thermal analysis

A TG–DTA Setaram Setsys Evolution thermal analyzer coupled with a mass spectrometer is used to follow the different steps of the synthesis process. The same equipment is transformed in a dilatometer by replacing the TG–DTA probe by a dilatomer one.

2.2.3. Microstructure

Powders and pellets are observed with a HITACHI S 2500 scanning electron microscope (SEM). Semi-quantitative analysis was performed using EDS technique with internal standards. More precise quantitative analysis is conducted by Cameca SX-50 electron microprobe, as in Ref. 28.

3. Results

3.1. Reaction scheme

The reagents in reaction (1) are commercial Aldrich products CeO_2 and $CaCO_3$. ThO_2 is provided from internal stocks. $LaPO_4$ is synthesized as described in Ref. 42: it consists of an aqueous precipitation from lanthanum nitrate and phosphorous acid aqueous solutions followed by a thermal treatment at 1250 °C for one night. Metaphosphate is synthesized by a dry high-temperature reaction between La_2O_3 and $NH_4H_2PO_4$ as described in Refs. 43, 44 and 45.

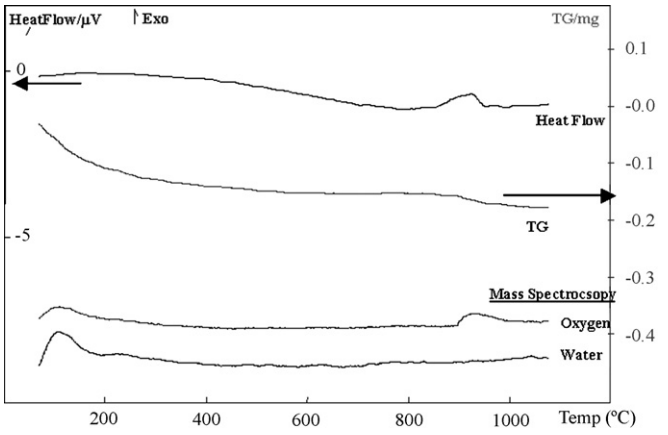

Fig. 1. DTA–TGA measurements of the reaction (2), coupled with a mass spectrometer.

The reaction (2) was monitored by a TG–DTA-mass spectrometer (Fig. 1), the mixture of precursors being heated at 10 °C/min in an air environment.

As shown by Fig. 1 only a slight evaporation of superficial water is observed at low temperature (below 200 °C). Between 900 and 975 °C, three phenomena occurred simultaneously:

- Evaporation of oxygen;
- Weight loss;
- Exothermic peak.

The weight loss due to oxygen evaporation corresponds exactly to the amount of oxygen expected from the reduction of Ce. This reduction should produce an endothermic peak, but we observed instead an exothermic peak on the DTA curve, attributed to the monazite-forming reaction, which produces an exothermic peak much larger than the endothermic peak corresponding to the reduction of Ce.

These results suggest that all precursors react simultaneously at about 900 °C: cerium oxide is reduced and reacts with metaphosphate and $LaPO_4$. This is in agreement with previous results[28] that showed that a reaction between metaphosphate and cerium oxide started at 1000 °C.

From previous work,[28] we know that thorium oxide reacts with metaphosphate between 1000 and 1100 °C. Therefore, in the reaction (1), we assumed that the calcium and the thorium are loaded into the orthophosphate structure in the same way, producing ssMB just above 1100 °C.

Those results are in agreement with Bregiroux et al.[26] would found in a similar process, formation of $CePO_4$ at 850 °C. However they showed that CeP_2O_7 formed as an intermediate step from CeO_2 and $NH_4H_2PO_4$. This phase was never seen in our work, nor in the work of Montel et al.[28]

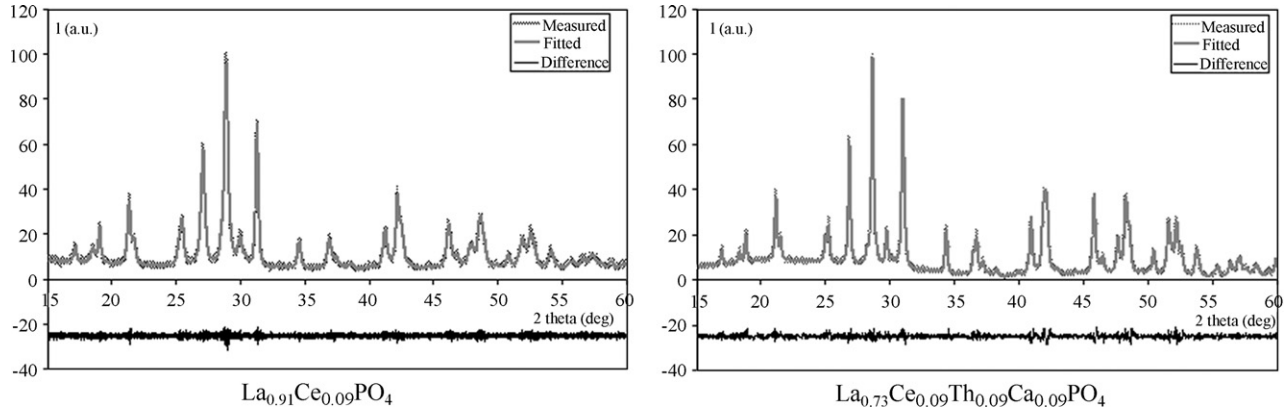

Fig. 2. X-ray pattern and FullProf fittings of monazite obtained with reaction (2) and monazite–brabantite obtained with reaction (1).

3.2. X-ray analysis

After an overnight heating at 1200 °C, the powders obtained from reactions (1) and (2) are still a single-phase, well-crystallized monazite–brabantite solid solution, as shown by the X-ray diffraction patterns (Fig. 2).

The unit-cell parameters of $La_{0.91}Ce_{0.09}PO_4$ and $La_{0.73}Ce_{0.09}Th_{0.09}Ca_{0.09}PO_4$ measured by a Rietveld routine with FullProf software[41] are given in Table 1, as well as the PDF reference cell parameters of $LaPO_4$,[46,47] $CePO_4$[46] and $Ca_{0.5}Th_{0.5}PO_4$.[48]

Assuming that lanthanides orthophosphates obey Vegard's law,[49] the theoretical unit-cell parameters can be calculated and compared to the experimental ones. $La_{0.91}Ce_{0.09}PO_4$ and $La_{0.73}Ce_{0.09}Th_{0.09}Ca_{0.09}PO_4$ should have unit-cell parameters of: ($a = 6.8274$ Å, $b = 7.0656$ Å, $c = 6.4999$ Å, $\beta = 103.2844°$) and ($a = 6.8062$ Å, $b = 7.0382$ Å, $c = 6.4847$ Å, $\beta = 103.367°$), respectively. The measured parameters are in total agreement with the expected values so we conclude that the compositions of the final powders correspond exactly to the desired compositions, as far as X-ray diffraction is concerned.

3.3. Sintering

In the previous work,[28] a procedure was defined to sinter pellets of ssMB with a geometrical density above 95% of the theoretical density. However,[50] this procedure fails to produce thorium-free monazite ($LaPO_4$ and $La_{0.91}Ce_{0.09}PO_4$) with a density above 85%. Bregiroux et al.[51] showed that, to obtain a density above 95%, a specific area of at least 17 m^2/g is necessary. Hikichi et al.[52,53] have found the same results on ball-milled powder: with a specific area of 52.8 m^2/g, they obtained a density up to 98%. However with the mixed-mill tool we used, we could not reach specific surface area higher than 7 m^2/g.

The difference in the sintering properties of Th-Ca bearing monazite compared to pure rare earth monazite is surprising. We attribute this feature to differences in the geometry of the nine-folded polyhedra. In LaO_9 and CeO_9, La–O and Ce–O length are about only 1% difference (0.03 Å for 2.56 Å),[46,47] whereas the Ca–O and Th–O[48] distances in CaO_9 and ThO_9 polyhedra are 0.1 Å shorter or longer than the La–O and Ce–O distances. Therefore, the pure monazite structure (containing only LaO_9 and CeO_9) should be more rigid than a monazite–brabantite structure, which contains four different polyhedra LaO_9, CeO_9, CaO_9 and ThO_9. This could explain the higher ability of ssMB to sinter and reach a high density compared to monazite.

In this work, only sintering of $La_{0.73}Ce_{0.09}Th_{0.09}Ca_{0.09}PO_4$ is studied. Powders obtained from reaction (1) are pounded and pressed using the following optimized procedure[28]:

- Milling 2 g of powder with a mixer-mill containing a zirconia ball at 25 Hz during 30 min.
- Compacting the powder at room temperature with a manual hydraulic one-axial press in a 10 mm diameter steel matrix.
- Sintering at room pressure, 1450 °C during 4 h.

From dilatometric studies; Montel et al.[28] defined an optimized thermal treatment consisting of heating in air at 10 °C/min. In the present study, we performed 5 additional dilatometric analyses with various conditions: air and argon environment, heating rates from 1 to 30 °C/min, from room temperature up to 1500 °C. The dilatometric curves and their derivative are shown in Fig. 3. Those results must be compared

Table 1
The cell parameter of $La_{0.91}Ce_{0.09}PO_4$ and $La_{0.73}Ce_{0.09}Th_{0.09}Ca_{0.09}PO_4$ and reference cell parameters.

Sample	a (Å)	b (Å)	c (Å)	β (°)
$La_{0.91}Ce_{0.09}PO_4$	6.8275(5)	7.0609(5)	6.5005(4)	103.310(4)
$La_{0.73}Ce_{0.09}Th_{0.09}Ca_{0.09}PO_4$	6.8088(4)	7.0407(4)	6.48774(3)	103.353(3)
$LaPO_4$[46]	6.8313(1)	7.0705(9)	6.5034(9)	103.270(1)
$CePO_4$[46]	6.788(1)	7.0163(8)	6.465(7)	103.430(1)
$Ca_{0.5}Th_{0.5}PO_4$[48]	6.7137(6)	6.9181(5)	6.4187(12)	103.732(27)

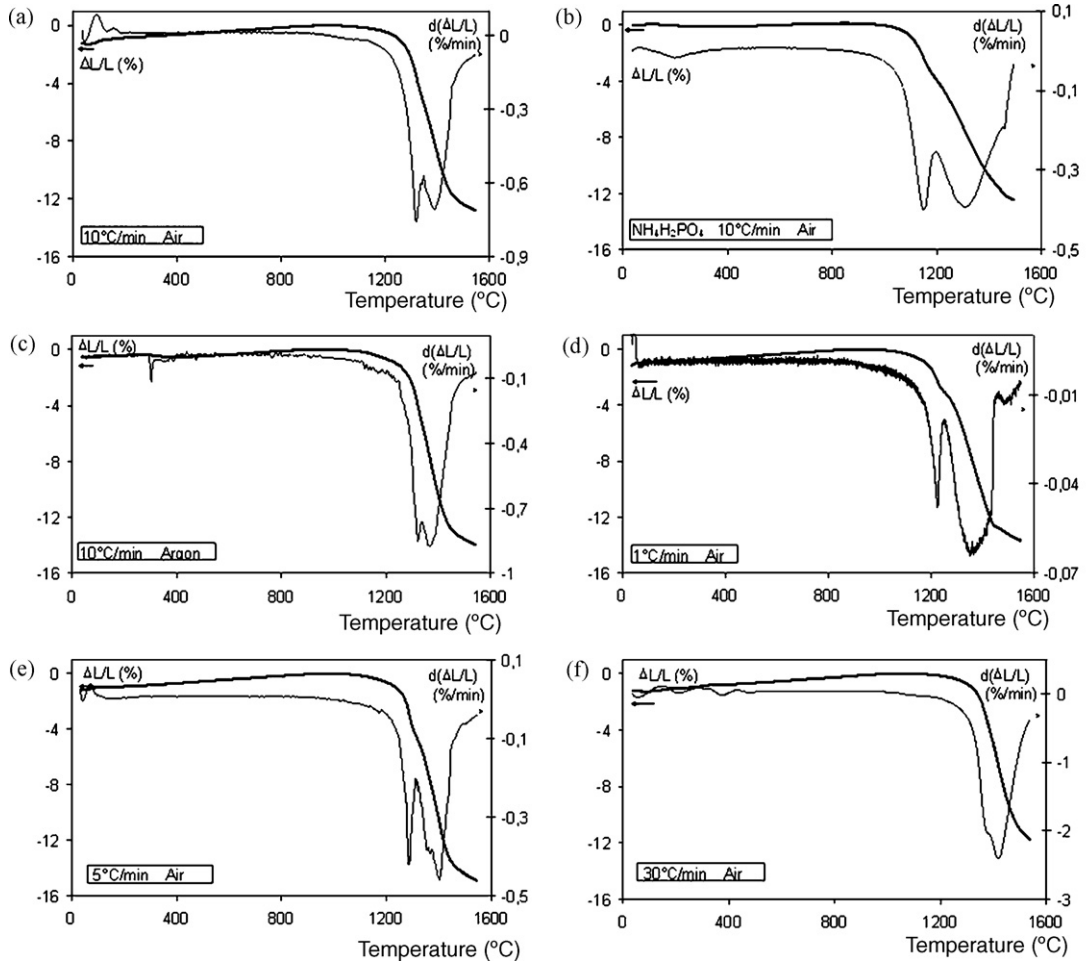

Fig. 3. Dilatometric curves of $La_{0.73}Ce_{0.09}Th_{0.09}Ca_{0.09}PO_4$ heated at 10 °C/min (a–c), 1 °C/min (d), 5 °C/min (e), and 30 °C/min (f), in air (a, b, d–f) and argon (c). The phosphorous reagent is metaphosphate (a, c, d–f) and ammonium dihydrogenophosphate (b).

with the previous dilatometric analysis,[28] performed with a sample synthesized with ammonium dihydrogenophosphate. At the end of the dilatometric analyses, all samples are polished with a 1 μm SiC suspension then heated during 5 min at 1425 °C, to enhance the grain boundary visualization. SEM images of the final sintered samples are shown in Fig. 4.

After an overnight thermal treatment at 1450 °C, the final geometrical density is always between 95 and 98% of the theoretical one. For $La_{0.73}Ce_{0.09}Th_{0.09}Ca_{0.09}PO_4$ heated at 10 °C/min in air (Fig. 4a), a 1% linear swelling is visible below 1000 °C. Shrinkage starts at 1100 °C and occurs in two steps (as shown by the derivative curves). The grains boundaries are well defined, with sharp edges and triple junctions, without any heterogeneity. The grain size varies from 1 to 10 μm with an average size of 6 μm. The low-temperature swelling ($T < 800$ °C), Fig. 3, is certainly due to an increase of the internal porosity, the most classic reason of this kind of phenomena.[54]

The most interesting feature is the presence of a two-step shrinkage above 1100 °C. The first step achieves a maximum (minimum of the derivative curve) at 1319 °C and the second one at 1391 °C. At 1500 °C, sintering is almost over. The final geometrical density of $La_{0.73}Ce_{0.09}Th_{0.09}Ca_{0.09}PO_4$ sintered at 10 °C/min in air is 91.3%. After an overnight thermal treatment at 1450 °C, the final geometrical density reaches the desired value, above 95%.

Bregiroux et al.[51] observed two mechanisms during shrinkage: the grain coalescence at lower temperature and the grain boundary diffusion at higher temperature. The coalescence determines the initial number of grains while the diffusion determines the final grain size.

3.4. Influence of the precursors

The dilatometric measurement of Montel et al.[28] on a sample synthesized with ammonium dihydrogenophosphate is reported in Fig. 3b for comparison. It displays some differences when compared to Fig. 3a, even if the final densities are almost the same (91.3 and 91.4%). No swelling occurs at low temperature for that sample, but the two steps of shrinkage also exist. The characteristic temperatures (minimum of the derivative curve) are lower than for ammonium-free sample, respectively, 1154 and 1313 °C, but the second step is more intense with ammonium dihydrogenophosphate than with metaphosphate. The grain size is also different, since many grains larger than 10 μm are present with ammonium dihydrogenophosphate (Fig. 4b).

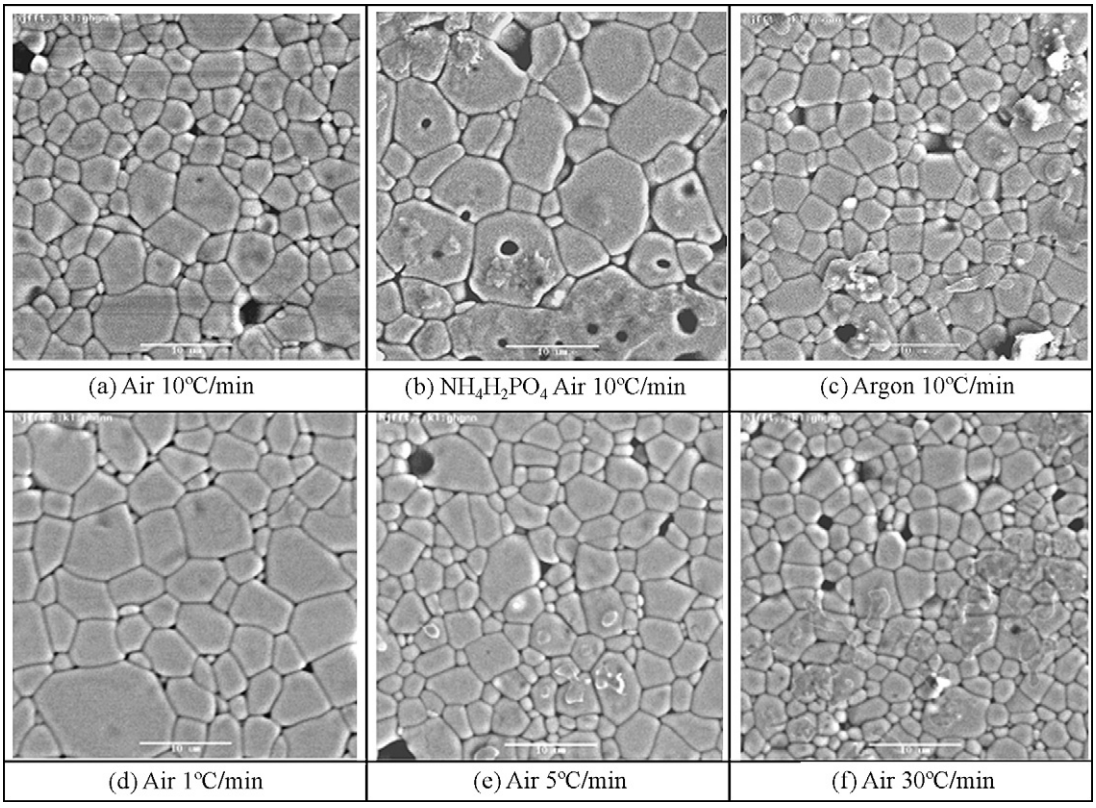

Fig. 4. SEM images, with a 2000 magnification and secondary electrons view of $La_{0.73}Ce_{0.09}Th_{0.09}Ca_{0.09}PO_4$ sintered in at 10 °C/min (a–c), 1 °C/min (d), 5 °C/min (e), and 30 °C/min (f), in air (a, b, d–f) and argon (c). The phosphorous reagent is metaphosphate (a, c, d–f) and ammonium dihydrogenophosphate (b).

The comparison between those two samples suggests that the second step of shrinkage corresponds to the grain growth. The more intense the second phenomenon, the bigger is the grain size, in agreement with the suggestion of Bregiroux[51] and Bernache-Assolant.[54]

3.5. Influence of the environment

The dilatometric curves and their derivative obtained at 10 °C/min in air (Fig. 3a) and in an argon environment (Fig. 3c) are similar. The difference in the shrinkage temperature is less than 10 °C and the intensity of each phenomenon is equivalent. The grain sizes are similar, as shown on the SEM images (Fig. 4a and c). It can be concluded that the gaseous environment does not influence the sintering processes of the solid solution.

3.6. Influence of the temperature rate

The measurements performed on samples heated at various temperature rates (d: 1 °C/min, e: 5 °C/min, f: 30 °C/min) are compared to the sample heated at 10 °C/min in Table 2.

The low-temperature swellings are identical, and the two high-temperature shrinkage steps are observed too. The temperature rate influences the low-temperature swelling and increases the sintering temperature. This effect is usually observed[55] and is related to the decrease in time for sintering to be activated.

The final geometrical densities are always between 91 and 95%. The intensity of shrinkage is reproducible in a 2% range. The most interesting point is the shapes of the curves and their derivatives, as well as their characteristic temperatures. At low-temperature rate (1 °C/min), the temperature difference between the two shrinkage steps is of 134 °C. The second step is large and intense. With increasing temperature rate, the distinction between the two steps becomes less visible, and the temperature difference drops from 134 °C to 52 °C.

The temperature rate influences the grain size, as clearly shown by SEM images (Fig. 4a, d–f). For a temperature rate of 1 °C/min, the grain size can reach 20 μm, with an average of 9 μm. For a temperature rate of 30 °C/min, the grain size varies from 0.5 to 8 μm with an average size of 2.5 μm. Those data agree with the assignment of the second shrinkage step to grain

Table 2
Geometrical densities, sintering phenomena 1 and 2 temperatures of $La_{0.73}Ce_{0.09}Th_{0.09}Ca_{0.09}PO_4$ heated at various temperature rate.

Sample	Temperature rate (°C/min)	Geometrical density (%)	T. phenom. 1 (°C)	T. phenom. 2 (°C)
a	1	95.1	1226	1360
d	5	93.3	1286	1378
e	10	91.3	1319	1391
f	30	93.9	1378	1420

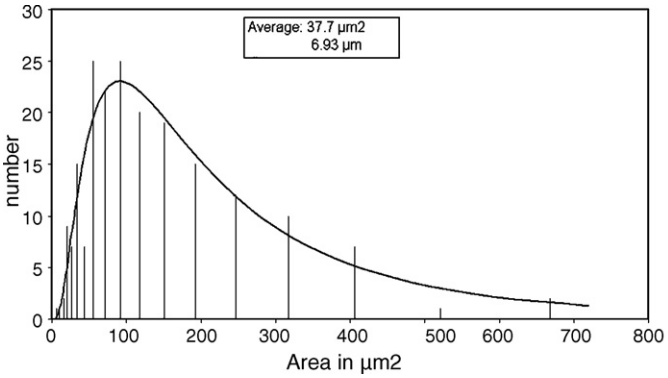

Fig. 5. Grains size distribution. The bars represent the observed distribution and the line is the fitted log-normal law.

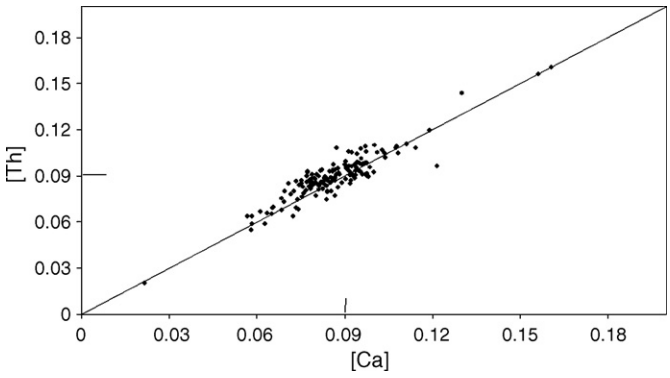

Fig. 6. Distribution of the ceramics compositions projected in the Ca–Th plane. The line is the 1/1 ratio. The 0.9 dash line correspond to the theoretical values.

boundary diffusion. The grain size is controlled by the grain growth mainly, which results from the grain boundary diffusion. Thus, the longer the sample is kept in the grain boundary diffusion temperature range, the bigger are the grain sizes. For a high-temperature rate, the sample remains in the 1100–1500 °C temperature range during 13 min, while for the minimum temperature rate, this duration is increased to 400 min. This confirms that the first shrinkage step corresponds to the grain coalescence and the second one the grain boundary diffusion, in agreement with Refs. 51, 54 and 55.

The average grain size is always less than 10 μm and, in all the cases, the final geometrical densities between 95 and 98% after an overnight thermal treatment.

3.7. Reproducibility

A batch of 10 pellets of $La_{0.73}Ce_{0.09}Th_{0.09}Ca_{0.09}PO_4$ was synthesized and sintered using a 10 °C/min temperature rate in air and with a 4 h heat treatment at 1450 °C.

The average density value is $\rho = 4.9(8)$ g/cm^3, corresponding to 97.4% of the theoretical value, with a standard deviation less than 0.01. The process described here is then highly reproducible, at least at the laboratory scale.

3.8. Grain size

The grain size distribution was measured by image processing on samples prepared according to the reference routine. A typical result of the grain size distribution measurement for 200 grains is shown in Fig. 5.

As for Ref. 28, the distribution is characterized by a log-normal law. The average area corresponds to 38 μm^2, which, with a spherical-shape grain assumption, correspond to an average equivalent diameter of 7 μm. This value is in agreement with the previous grain size of 6 μm (Fig. 4a) for a sample synthesized with the same process and sintered at the same heating rate. The increase in size, compared with sample studied in the dilatometric analysis (Fig. 4a), is related to the 4 h 1450 °C stage after heating necessary to increase the density.

3.9. Chemical composition

With the electron microprobe used in Ref. 28, using the same analytical routine, we determined the chemical composition of 71 spots selected on 13 samples synthesized and sintered using a 10 °C/min in air environment and with a 4 h duration at 1450 °C.

The amounts of lanthanum, cerium, calcium and thorium correspond, in all the cases, to the desired values, with a dispersion less than 4% for La and Ce, 3% for P (relative%), only slightly higher than the accuracy of the electron microprobe (1–2 relative%). The Ca and Th are distributed more heterogeneously (11 relative%). The Ca and Th distributions are reported in Fig. 6.

It can be noticed that the compositions are distributed along the 1/1 line in the Ca–Th diagram, with a very limited thorium excess, showing that, in ssMB, Th and Ca remains spatially linked. Those data show that the addition of brabantite ($Ca_{0.5}Th_{0.5}PO_4$) into monazite is quite heterogeneous. In reaction (1), 80% of monazite, $LaPO_4$, is already part of the precursor. Contrary to the process using ammonium dihydrogenophosphate,[28] the incorporation of cations (Ca–Th and Ce) does not occur simultaneously at high temperature but are incorporated in an already existing $LaPO_4$. Due to the slow kinetics of Ca and Th diffusion in the monazite,[57] it is almost impossible to obtain finally an homogeneous distribution of Ca and Th. If MBss is used as an actual waste-form, this should be taken into account in order to avoid local concentrations of actinides.

The slight excess in Th compared to Ca was already observed by Cuney et al.[56] who suggested that the orthophosphate could stand some $3Th^{4+} \Leftrightarrow 4La^{3+} + 1$ lacuna substitution. This phenomenon was not observed by Montel et al.[28]

4. Conclusions

A monazite–brabantite solid solution can be synthesized and sintered by a high-temperature solid-state reaction with a very limited gas emission. The use of metaphosphate $La(PO_3)_3$ and LaPO4, instead of ammonium dihydrogenophosphate,[28] as phosphorous reagent, simplifies the reaction scheme, and only minor CO_2 and O_2 are emitted during the synthesis.

The final product is perfectly single-phased and well crystallized, but the product is less homogeneous in terms of

brabantite–monazite distribution. The final densities are always above 95% of the theoretical one, whatever the gaseous environment and the temperature rate are.

The procedure is highly reproducible and directly usable in a radioactive environment such as glove box and hot cell.

Acknowledgements

Authors thank GDR NOMADE, part of the PACE CNRS program for supporting this work. Many thanks are due to V. Picot for her help on sintering comprehension, Ph De Parseval for technical support on microprobe, D. Gorand for assistance on SEM, G. Hernandez for his support on thermal analysis and Mark Jessell for his help in the English writing.

References

1. Boatner, L. A. and Sales, B. C., Monazite. In *Radioactive Waste Forms for the Future*, ed. W. Lutze and R. C. Ewing. Elsevier, Amsterdam, 1988, pp. 495–564.
2. Aloy, A. S., Kovarskaya, E. N., Koltsova, T. I., Samoylov, S. E., Rovnyi, S. I., Medvedev, G. M. *et al.*, Immobilization of AM-241, formed under plutonium metal conversion into monazite-type ceramics. In *8th International Conference on Environmental Management*, 2001. pp. 1833–1839.
3. Bamberger, C. E., Haire, R. G., Begun, G. M. and Ellingboe, L. C., Synthesis and characterization of phosphates containing alkali metals and plutonium or lanthanides. *Inorg. Chim. Acta*, 1984, **95**(1), 49–56.
4. Tabuteau, A., Pagès, M., Livet, J. and Musikas, C., Monazite-like phases containing transuranium elements (neptunium and plutonium). *J. Mater. Sci. Lett.*, 1988, **7**(12), 1315–1317.
5. Anderson, E. B. and Burakov, B. E., *Ceramics for the Immobilization of Plutonium and Americium: Current Progress of R&D of the V.G. Khlopin Radium Institute, Unconventional Approaches to Nanostructures with Applications in Electronics, Photonics, Information Storage and Sensing*, 2004, pp. 207–212.
6. Montel, J. M., Kornprobst, J. and Vielzeuf, D., Preservation of old U–Th–Pb ages in shielded monazite: example from the Beni Bousera Hercynian kinzigites (Morocco). *J. Metam. Geol.*, 2000, **18**(3), 335–342.
7. Guimei, Y. and Liangchao, Z., The first discovery of monazite-(Nd) in China. *Acta Min. Sin.*, 1988, **8**(1), 25–29.
8. Mathieu, R., Zetterstrom, L., Cuney, M., Gauthier-Lafaye, F. and Hidaka, H., Alteration of monazite and zircon and lead migration as geochemical tracers of fluid paleocirculations around the Oklo-Okelobondo and Bangombe natural nuclear reaction zones (Franceville basin, Gabon). *Chem. Geol.*, 2001, **171**(3), 147–171.
9. Andrehs, G. and Heinrich, W., Experimental determination of REE distributions between monazite and xenotime: potential for temperature-calibrated geochronology. *Chem. Geol.*, 1998, **149**(1), 83–96.
10. Montel, J. M., Foret, S., Veschambre, M., Nicollet, C. and Provost, A., Electron microprobe dating of monazite. *Chem. Geol.*, 1996, **131**(1), 37–53.
11. Seydoux-Guillaume, A. M., Paquette, J. L., Wiedenbeck, M., Montel, J. M. and Heinrich, W., Experimental resetting of the U–Th–Pb systems in monazite. *Chem. Geol.*, 2002, **191**(1), 165–181.
12. Bois, L., Guittet, J., Carrot, F., Trocellier, P. and Gautier-Soyer, M., Preliminary results on the leaching process of phosphate ceramics, potential hosts for actinide immobilization. *J. Nucl. Mater.*, 2001, **297**(2), 129–137.
13. Guo, D., Fu, X., Tang, J., Jiang, L., Liu, X. and Byrne, R. H., Rare earth and yttrium phosphate solubilities in aqueous solution. *Geochim. Cosmochim. Acta*, 1997, **61**(8), 1625–1633.
14. Poitrasson, F., Oelkers, E. H., Schott, J. and Montel, J. M., Experimental determination of synthetic $NdPO_4$ monazite end-member solubility in water from 21 °C to 300 °C: implications for rare earth element mobility in crustal fluids. *Geochim. Cosmochim. Acta*, 2004, **68**(10), 2207–2221.
15. Poitrasson, F., Chenery, S. and Bland, D. J., Contrasted monazite hydrothermal alteration mechanisms and their geochemical implications. *Earth Planet. Sci. Lett.*, 1996, **145**, 79–96.
16. Oelkers, E. H. and Poitrasson, F., An experimental study of the dissolution stoichiometry and rates of a natural monazite as a function of temperature from 50 to 230 °C and pH from 1.5 to 10. *Chem. Geol.*, 2002, **191**(1), 73–87.
17. Papoulis, D., Tsolis-Katagas, P. and Katagas, C., Monazite alteration mechanisms and depletion measurements in kaolins. *Appl. Clay Sci.*, 2004, **24**, 271–285.
18. Ewing, R. C., Weber, W. J. and Clinard, F. W., Radiation effects in nuclear waste forms for high-level radioactive waste. *Progr. Nucl. Energy*, 1995, **29**(2), 63–127.
19. Weber, W. J., Ewing, R. C., Catlow, C. R. A., Diaz de la Rubia, T., Hobbs, L. W., Kinoshita, C. *et al.*, Radiation effects in crystalline ceramics for the immobilization of high-level nuclear waste and plutonium. *J. Mater. Res.*, 1998, **13**(6), 1434–1484.
20. Meldrum, A., Boatner, L. A. and Ewing, R. C., A comparison of radiation effects in crystalline ABO_4-type phosphates and silicates. *Miner. Mag.*, 2000, **64**(2), 185–194.
21. Burakov, B. E., Yagovkina, M. A., Garbuzov, V. M., Kitsay, A. A. and Zirlin, V. A., Self-irradiation of monazite ceramics: contrasting behavior of $PuPO_4$ and (La, Pu)PO_4 doped with Pu-238. In *Scientific Basis for Nuclear Waste Management XXVIII, vol. 824*. MRS, 2004, pp. 219–224.
22. Meldrum, A., Boatner, L. A., Weber, W. J. and Ewing, R. C., Radiation damage in zircon and monazite. *Geochim. Cosmochim. Acta*, 1998, **62**(14), 2509–2520.
23. Meldrum, A., Boatner, L. A. and Ewing, R. C., Displacive radiation effects in the monazite- and zircon-structure orthophosphates. *Phys. Rev. B*, 1997, **56**, 13805–13814.
24. Seydoux-Guillaume, A. M., Wirth, R., Nasdala, L., Gottschalk, M., Montel, J. M. and Heinrich, W., An XRD, TEM and Raman study of experimentally annealed natural monazite. *Phys. Chem. Miner.*, 2002, **29**(4), 240–253.
25. Terra, O., Dacheux, N., Audubert, F. and Podor, R., Immobilization of tetravalent actinides in phosphate ceramics. *J. Nucl. Mater.*, 2006, **352**, 224–232.
26. Bregiroux, D., Terra, O., Audubert, F., Dacheux, N., Serin, V., Podor, R. *et al.*, Solid-state synthesis of monazite-type compounds. *Sol. Stat. Sci.*, 2007, **9**(5), 432–439.
27. Terra, O., Audubert, F., Dacheux, N., Guy, C. and Podor, R., Synthesis and characterization of thorium-bearing britholites. *J. Nucl. Mater.*, 2006, **354**, 49–65.
28. Montel, J. M., Glorieux, B., Seydoux-Guillaume, A. M. and Wirth, R., Synthesis and sintering of a monazite–brabantite solid solution ceramics for nuclear waste storage. *J. Phys. Chem. Solids*, 2006, **67**, 2489–2500.
29. Glorieux, B., Picot, V., Deschanels, X., Jorion, F., Montel, J. M. and Matecki, M., Confinement of plutonium and thorium in monazite/brabantite, in view of actinides. *Recent Advances in Actinide Science*. RSC Publishing, 2006, pp. 331–333.
30. Glorieux, B., Jorion, F., Montel, J. M., Deschanels, X., Matecki, M. and Coutures, J. P., Investigation of cerium, thorium and plutonium-239 conditioning in monazite and brabantite matrices: synthesis and characterization. In *Proceedings, ATALANTE 2004, 032-04*, 2004.
31. Glorieux, B., Berjoan, R., Matecki, M., Kammouni, A. and Perarnau, D., X-ray photoelectron spectroscopy analyses of lanthanides phosphates. *Appl. Surf. Sci.*, 2007, **253**, 3349–3359.
32. Deschanels, X., Picot, V., Glorieux, B., Jorion, F., Peuget, S., Roudil, D. *et al.*, Plutonium incorporation into phosphate and titanate ceramics for minor actinide containment. *J. Nucl. Mater.*, 2006, **352**, 233–240.
33. Podor, R., Cuney, M. and Nguyen, T. C., Experimental study of the solid solution between monazite-(La) and $(Ca_{0.5}U_{0.5})PO_4$ at 780 degrees C and 200 MPa. *Am. Miner.*, 1995, **80**, 1261–1268.
34. Onoda, H., Nariai, H., Maki, H. and Motooka, I., Syntheses of various rare earth phosphates from some rare earth compounds. *Mater. Chem. Phys.*, 2002, **73**(1), 19–23.
35. Fujishiro, Y., Ito, H., Sato, T. and Okuwaki, A., Synthesis of monodispersed $LaPO_4$ particles using the hydrothermal reaction of an La(EDTA)-chelate precursor and phosphate ions. *J. Alloys Compd.*, 1997, **252**(1), 103–109.

36. Terra, O., Clavier, N., Dacheux, N. and Podor, R., Preparation and characterization of lanthanum–gadolinium monazites as ceramics for radioactive waste storage. *New J. Chem.*, 2003, **27**, 957–967.
37. Abraham, M. M., Boatner, L. A., Quinby, T. C., Thomas, D. K. and Rappaz, M., Preparation and compaction of synthetic monazite powders. *Radioactive Waste Manage.*, 1980, **1**(2), 181–191.
38. Boatner, L. A., Synthesis, structure and properties of monazite, pretulite, and xenotime. *Rev. Mineral. Geochem.*, 2002, **48**, 87–121.
39. Carron, M. K., Naeser, C. R., Rose, H. J. and Hildebrand, F. A., Fractional precipitation of rare earth with phosphoric acid. *US Geol. Surv. Bull.*, 1958, **1036**, 253–275.
40. Lucas, S., Champion, E., Penot, C., Leroy, G. and Bernache-Assolant, D., Synthesis and characterisation of rare earth phosphate powders. *Key Eng. Mater.*, 2002, **206–213**, 47–50.
41. Roisnel, T. and Rodríguez-Carvajal, J., WinPLOTR: Windows tool for powder diffraction patterns analysis, Materials Science Forum. In *Proceedings of the Seventh European Powder Diffraction Conference (EPDIC 7)*, ed. R. Delhez and E. J. Mittenmeijer, 2000, p. 118.
42. Glorieux, B., Matecki, M., Fayon, F., Coutures, J. P., Palau, S., Douy, A. *et al.*, Study of lanthanum orthophosphates polymorphism, in view of actinide conditioning. *J. Nucl. Mater.*, 2004, **326**, 156–162.
43. Park, H. D. and Kreidler, E. R., Phase equilibria in the system La_2O_3–P_2O_5. *J. Am. Ceram. Soc.*, 1984, **67**(1), 23–26.
44. Serra, J. J., Coutures, J., Rouanet, A., Dexpert, H. and Caron, G., Synthesis, characterization, and thermal stability of rare earth oxyphosphates. *Rev. Int. Haut. Temp. Refr.*, 1978, **15**(4), 287–313.
45. Matuszewski, J., Kropiwnicka, J. and Znamierowska, T., The crystal structure of lanthanum metaphosphate LaP_3O_9. *J. Sol. Stat. Chem.*, 1988, **75**(2), 285–290.
46. Ni, Y., Hughes, J. M. and Mariano, A. N., Crystal chemistry of the monazite and the xenotime structure. *Am. Mineral.*, 1995, **80**, 21–26.
47. Mullica, D. F., Milligan, W. O., Grossie, D. A., Beall, G. W. and Boatner, L. A., Ninefold coordination in $LaPO_4$: pentagonal interpenetrating tetrahedral polyhedron. *Inorg. Chim. Acta*, 1984, **95**(4), 231–236.
48. Terra, O., *Incorporation d'actinides tétravalents dans trios matrices phosphates: britholite, monazite/brabantite et phosphate-diphosphate de thorium (PDT)*, PhD Thesis of Université Paris-Sud-11, IPNO-T-05-03, 2005.
49. Montel, J. M., Devidal, J. L. and Avignant, D., X-ray diffraction study of brabantite–monazite solid solutions. *Chem. Geol.*, 2002, **191**(1), 89–104.
50. D. Bregiroux, *Synthèse par voie solide et frittage de céramiques à structure monazite. Application au conditionnement des actinides mineurs*, PhD Thesis, Univ. Limoges, France, 2005.
51. Bregiroux, D., Lucas, S., Champion, E., Audubert, F. and Bernache-Assollant, D., Sintering and microstructure of rare earth phosphate ceramics $REPO_4$ with RE = La, Ce or Y. *J. Eur. Ceram. Soc.*, 2006, **26**, 279–287.
52. Hikichi, Y., Ota, T. and Hattori, T., Thermal, mechanical and chemical properties of sintered monazite–(La, Ce, Nd or Sm). *Mineral. J.*, 1997, **19**(3), 123–130.
53. Hikichi, Y. and Ota, T., Sintering and properties of monazite-type RPO_4 (R = La, Ce, Nd or Sm). *Phosp. Res. Bull.*, 1996, **6**, 175–181.
54. Bernache-Assollant, D., *Chimie-Physique du frittage*. Edition Forceman, Paris, France, 1993.
55. Chu, M. Y., Rahaman, M. N., De Jonghe, L. C. and Brook, R., Effect of heating rate on sintering and coarsening. *J. Am. Ceram. Soc.*, 1991, **74**(6), 1217–1225.
56. Cuney, M. and Mathieu, R., Extreme light rare earth element mobilization by diagenetic fluids in the geological environment of the Oklo natural reactor zones, Franceville basin, Gabon, *Geology*, 2000, **28**(8), 743–746.
57. Gardes, E., Jaoul, O., Montel, J. M., Seydoux-Guillaume, A. M. and Wirth, R., Pb diffusion in monazite: An experimental study of Pb + Th = 2Nd interdiffusion. *Geochim. Cosmochim. Acta*, 2006, **70**, 2325–2336.